Structure and Expression of Propanediol Utilization Microcompartments in *Acetonema longum*

Elitza I. Tocheva,[a] Eric G. Matson,[c] Sarah N. Cheng,[a] Wesley G. Chen,[a*] Jared R. Leadbetter,[c] Grant J. Jensen[a,b]

Division of Biology and Biological Engineering, California Institute of Technology, Pasadena, California, USA[a]; Howard Hughes Medical Institute, California Institute of Technology, Pasadena, California, USA[b]; Ronald and Maxine Linde Center for Global Environmental Science, California Institute of Technology, Pasadena, California, USA[c]

Numerous bacteria assemble proteinaceous microcompartments to isolate certain biochemical reactions within the cytoplasm. The assembly, structure, contents, and functions of these microcompartments are active areas of research. Here we show that the Gram-negative sporulating bacterium *Acetonema longum* synthesizes propanediol utilization (PDU) microcompartments when starved or grown on 1,2-propanediol (1,2-PD) or rhamnose. Electron cryotomography of intact cells revealed that PDU microcompartments are highly irregular in shape and size, similar to purified PDU microcompartments from *Salmonella enterica* serovar Typhimurium LT2 that were imaged previously. Homology searches identified a 20-gene operon in *A. longum* that contains most of the structural, enzymatic, and regulatory genes thought to be involved in PDU microcompartment assembly and function. Transcriptional data on PduU and PduC, which are major structural and enzymatic proteins, respectively, as well as imaging, indicate that PDU microcompartment synthesis is induced within 24 h of growth on 1,2-PD and after 48 h of growth on rhamnose.

Bacterial microcompartments are small, cytoplasmic, organelle-like bodies consisting of a thin, selectively permeable proteinaceous shell that surrounds a cluster of enzymes. Together, these isolate certain metabolic pathways away from the rest of the cytoplasm. Microcompartments may increase metabolic efficiency by concentrating enzymes and substrates, inhibiting nonproductive side reactions, or sequestering toxic by-products (1, 2). The best-studied microcompartments are the "carboxysomes" that sequester ribulose 1,5-bisphosphate carboxylase/oxygenase (RubisCO) and facilitate carbon fixation (3, 4). After early electron microscopy images of carboxysomes revealed their general size and shape (5), crystal structures of the shell proteins led to pseudoatomic models of carboxysomes as irregular polyhedra with hexagonally packed faces joined at the vertices by pentagonal disclinations (6, 7). In the case of carboxysomes, it was also recently shown that the RubisCO enzymes destined to be internalized cluster together and then nucleate the assembly of the shell (8). Electron cryotomography (ECT) (9) of purified carboxysomes (10) and then of intact cells producing carboxysomes (11) has shown that while purification enriches for more-nearly-icosahedral shapes, carboxysomes inside cells are more heterogeneous, exhibit ordered layers of enzymes packed against the shell, and harbor small internal storage granules as well as elaborate connections to larger, external storage granules (11).

In addition to carboxysomes, there are several other types of bacterial microcompartments, including propanediol utilization (PDU) and ethanolamine microcompartments (12, 13). Whether or not all microcompartments share similar assembly and structural features remains unclear. Projection images of plastic-embedded sections of PDU and ethanolamine microcompartments from *Salmonella enterica* and *Lactobacillus reuteri* have shown that these are also irregular polyhedra with thin shells (12, 14).

We recently discovered microcompartments in another organism, *Acetonema longum*, which is a strictly anaerobic, acetogenic bacterium found in the gut of the phylogenetically lower wood-feeding termite *Pterotermes occidentis* (15). In addition to using H$_2$ plus CO$_2$ as a source of energy and carbon, this bacterium can use a variety of organic carbon sources to support its growth. *A. longum* is unusual in that while it affiliates phylogenetically with *Clostridia*, within the phylum *Firmicutes*, and can sporulate, it is a *bona fide* Gram-negative species with both an inner and an outer membrane (15, 16). In our previous study, aimed at characterizing sporulation in *A. longum*, we observed microcompartments in some but not all sporulating cells (16). Here we identify the microcompartments in *A. longum* as PDU microcompartments, identify the operon responsible for their synthesis, structurally characterize them three-dimensionally (3-D) in their native state within intact cells by ECT, and explore the timing of their assembly when *A. longum* is grown on different carbon sources.

MATERIALS AND METHODS

Identification of PDU-associated genes. Sequences for the genes of structural proteins and enzymes associated with PDU microcompartments were obtained from the complete genome sequence of *Salmonella enterica* serovar Typhimurium LT2. These *S. enterica* genes were used to conduct BLAST (17) searches for homologs in the genome sequence of *A. longum* within the RAST annotation environment (18). *A. longum* homologs of *S. enterica* genes were used to conduct reciprocal BLAST searches against the NCBI database to confirm the putative gene identities.

Quantitative reverse transcription-PCR (qRT-PCR) of *pduC* and *pduU* transcripts. Total RNAs were prepared from 5-ml cultures of *A. longum* cells by first stabilizing each sample with 2 volumes of RNA Protect reagent for bacteria (Qiagen) and then extracting the samples with RNeasy extraction kits (Qiagen) according to the manufacturer's instructions. To ensure removal of DNA from the samples, the RNeasy extraction

FIG 1 Electron cryotomography of a sporulating *A. longum* cell reveals the presence of microcompartments. Arrows point to structures in the prespore and mother cell consistent with features of bacterial microcompartments. Additional features, such as membrane vesicles inside and outside the cell, are also apparent. The panel is a 20-nm-thick tomographic slice through a 3-D reconstruction. Bar, 200 nm.

was performed twice. The first extraction included a 10-min on-column DNA digestion step using Qiagen DNase. This was followed by a 30-min off-column DNase digestion at 37°C, using RQ1 RNase-free DNase (Promega Corp., Madison, WI), followed by a stop reaction performed according to the manufacturer's directions. Finally, the sample was run through a second RNeasy column without further DNase digestion. RNA was collected and quantified using absorbance values and ratios at 260 nm and 280 nm. All RNA samples had concentrations between 50 ng/μl and 400 ng/μl and 260-nm/280-nm absorbance ratios of approximately 2. Total RNA (500 ng) from each sample was converted into total cDNA by using am iScript randomly primed cDNA synthesis kit (Bio-Rad Laboratories, Inc., Hercules, CA).

The transcription levels of *pduC* and *pduU* were monitored by quantitative PCR using IQ PCR supermix reagent from Life Technologies and gene-specific primers. The forward and reverse primers used for *pduC* were 5′-GATATCGCCAAAATGCTGGT and 5′-ACCACGTTCATGGT GTTGAA, respectively, and the forward and reverse primers for *pduU* were 5′-GGGAGTTATGCGACAAGTT and 5′-GGTCCAGAAAGCCTA TTTCC, respectively. Transcription levels of *clpX*, which encodes the housekeeping enzyme caseinolytic peptidase X, were used as an endogenous control for the cDNA concentration. Forward and reverse primers for *clpX* were 5′-CGTTGACGGAGTCGGTTAT and 5′-ACAATCCCTT TTTCGGCTTT, respectively.

ECT sample preparation, data collection, and analysis. Cells were frozen and imaged as described previously (16). Data were collected from −60° to 60°, with an angular step of 1°, a total dose of 200 e⁻/Å², a defocus value of 10 μm, and a pixel size of 2 nm on a 300-kV FEG G2 Polara transmission electron microscope (TEM) equipped with a lens-coupled 4k-by-4k Ultracam (Gatan, CA) and an energy filter. Data were collected automatically with the UCSF tomography package (19) and reconstructed using the IMOD software package (20). Manual segmentation of the PDU microcompartments was done using Amira (Mercury Computer Systems). Every 2-D slice was contoured individually to ultimately represent a 3-D surface of the whole microcompartment. The surface was additionally smoothened for visual representation.

Culture growth conditions. *Acetonema longum* APO-1 cells were grown as described previously (16), with the following modifications. Cells were grown anaerobically in 4YACo medium (21) supplemented with different carbon sources at a 20 mM concentration. In order to test how well *A. longum* grew on 1,2-propanediol (1,2-PD), cultures were started on a combination of glucose and H₂ plus CO₂, a condition that enhances growth of the strain, presumably through mixotrophism (22) and as described previously (16). The carbon sources tested were glucose, rhamnose, 1,2-PD, and H₂ plus CO₂ (control). All cultures were grown in the presence of 80% H₂ plus 20% CO₂ to support mixotrophic growth. Cultures grown in this way were concentrated by gentle centrifugation
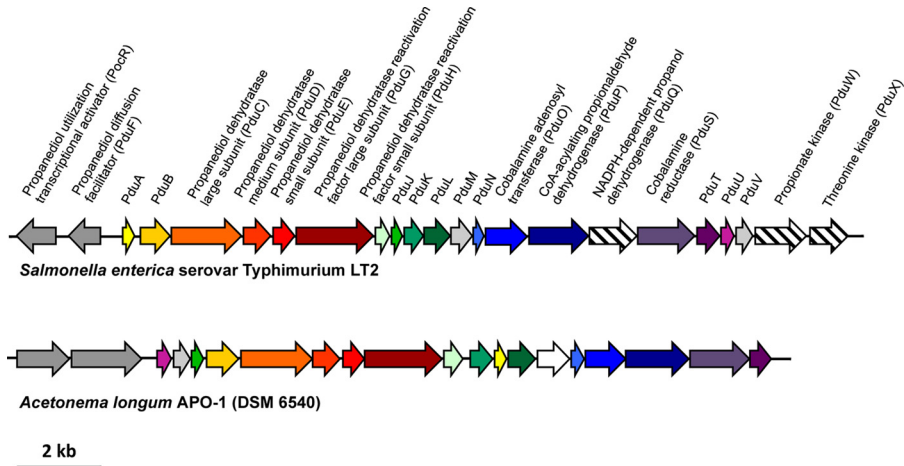

FIG 2 Genes for propanediol utilization (*pdu*). The genome context of genes involved in forming the PDU microcompartment in *A. longum* (bottom) is compared to the *pdu* operon of *S. enterica* (top). Homologous genes are depicted by the same color. Transcriptional regulators are shown in gray. Striped arrows denote genes in *S. enterica* found elsewhere in the genome of *A. longum*. Genes of unknown function and homology are shown in white.
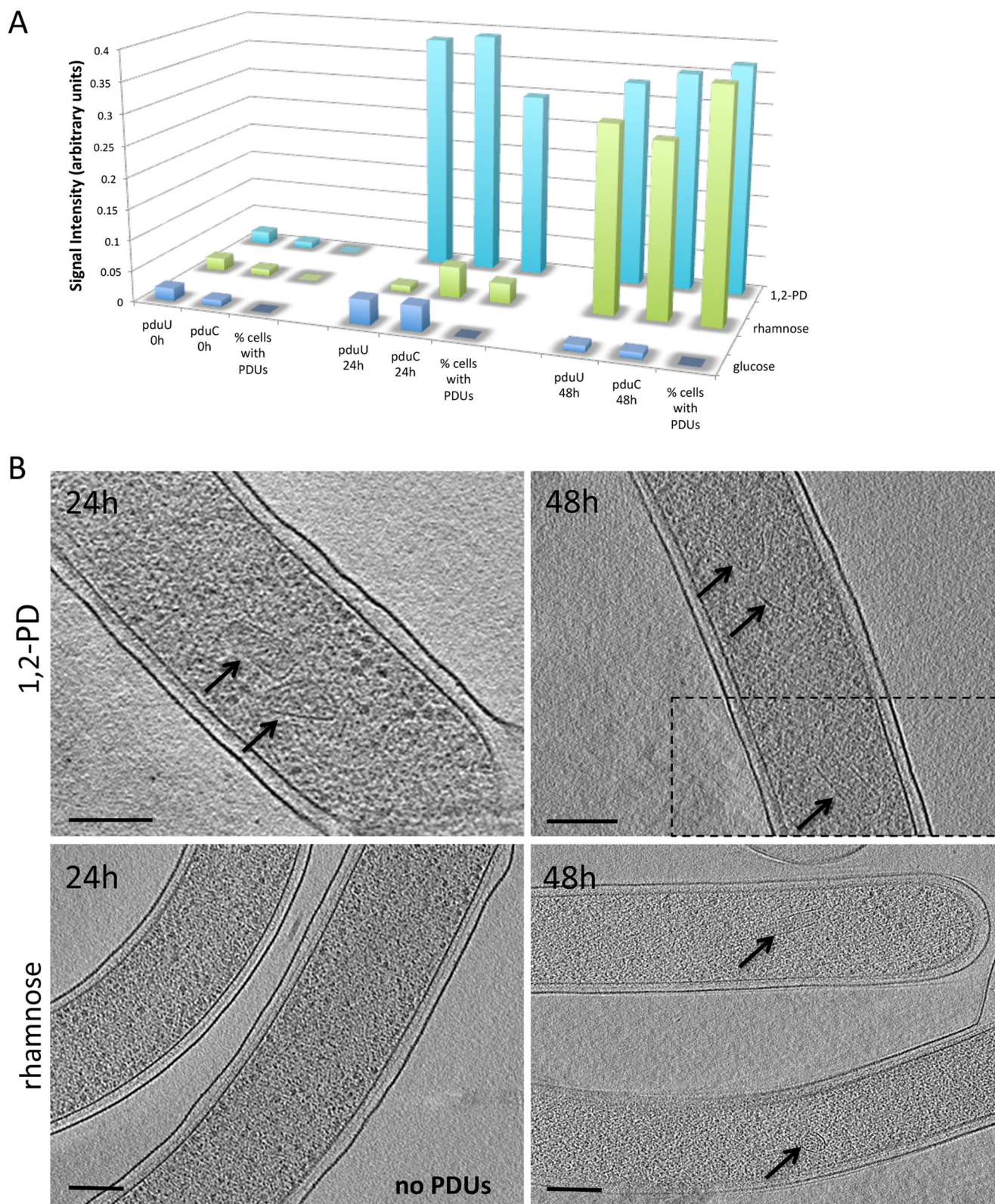
FIG 3 Transcriptional and structural studies of two major genes associated with 1,2-PD utilization in *A. longum*. (A) Transcriptional and translational levels of *pduU*, a gene encoding the microcompartment shell protein PduU, and *pduC*, encoding a subunit of the PduCDE enzyme comprising the coenzyme B_{12}-dependent diol dehydratase. Samples were collected at 0 h, 24 h, and 48 h, and the signal intensities were compared to those of the samples collected at 0 h. The percentages of cells documented to have PDU microcompartments were normalized to 0.4. (B) Tomographic data collected at the same time points as the transcriptional data reveal the presence of PDU microcompartments after 48 h of growth on rhamnose and within 24 h of growth on 1,2-PD. The dashed line in the top right panel indicates a different slice through the same tomogram. Bars, 150 nm.
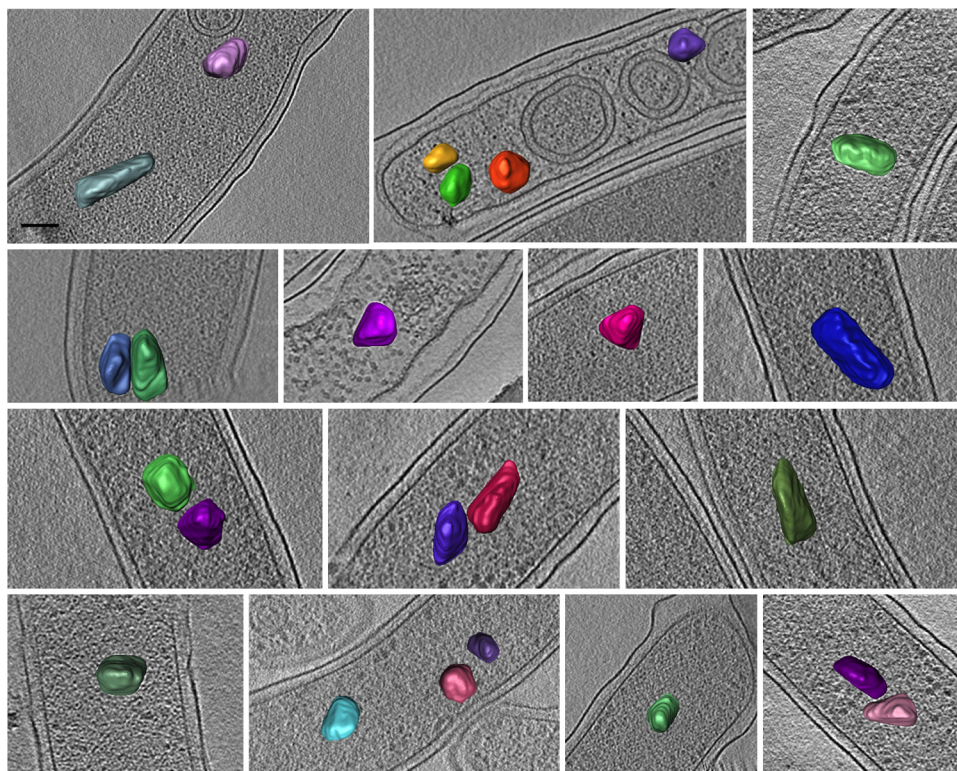
FIG 4 Size and shape variability of intracellular PDU microcompartments in *A. longum*. Cryotomograms of cells grown under different conditions were manually rendered for visualization purposes. Sections of different cells have their microcompartments depicted in different colors. Each panel is a 20-nm-thick tomographic slice through a 3-D reconstruction. Bar, 50 nm.

(approximately $3,000 \times g$) under anaerobic conditions to remove residual glucose and H_2 and were then inoculated into media containing a variety of carbon sources provided at a 20 mM concentration. Cultures were incubated at 27°C in anaerobic Hungate culture tubes (18-mm diameter), and optical densities at 600 nm (OD_{600}) were recorded directly through the tubes. Cells were harvested for imaging and PCR analysis at the 24-h and 48-h time points. The growth of the cultures was also monitored by measuring the OD_{600} over 8 days.

Only a few bacterial species have been found to grow on 1,2-PD as the sole carbon and energy source, and studies have shown that growth on 1,2-PD depends on the presence of a specific terminal electron acceptor (12, 23, 24). We therefore tested growth of *A. longum* on 1,2-PD by providing an assortment of potential electron acceptors at a 10 mM concentration. To force the cells to use 1,2-PD as the electron donor in the presence of different terminal electron acceptors, the headspace of the Hungate tubes and the growth medium was flushed with a gas mixture of 80% N_2 and 20% CO_2. When *S. enterica* was grown similarly on 1,2-PD under anaerobic conditions, tetrathionate was required as an electron acceptor (provided at a 10 mM concentration) for growth on 1,2-PD (25). Therefore, in addition to tetrathionate (which supports growth of *S. enterica* on 1,2-PD), we tested nitrate (a strong inorganic electron acceptor), fumarate (a widely utilized organic electron acceptor), and glycine (an electron acceptor utilized by some other members of the phylum *Firmicutes* in Stickland reactions).

RESULTS

In our previous study of *A. longum* sporulation (16), microcompartments were observed in just ~2.5% of the cells imaged. The microcompartments were present in both immature spores and mother cells (Fig. 1) and were clearly smaller and less regularly shaped and contained smaller enzymes than the RubisCO-con-

taining carboxysomes of chemotrophic, carbon-fixing bacteria imaged before by ECT in our lab (11, 26).

PDU-associated genes in *A. longum* form a putative operon. In order to identify what kind of microcompartments were formed by *A. longum*, we searched for homologs of two conserved carboxysome shell proteins, CcmK2 and CcmK4. The only homologous proteins in *A. longum* were found to be encoded within an operon also containing the genes for PduCDE, the main enzyme for 1,2-PD catabolism, suggesting that these were PDU microcompartments. The other 16 genes in the operon were then identified as encoding homologs of all of the major structural and enzymatic components associated with PDU microcompartments in *Salmonella enterica* serovar Typhimurium LT2, the model organism for PDU microcompartment structure and function (12, 27, 28) (Fig. 2). The operon was flanked upstream by genes predicted to encode a putative sensor kinase and a DNA-binding response regulator likely involved in regulating the expression of the PDU genes. Three PDU genes found in *S. enterica* were not found within the gene cluster in *A. longum*. Of these, the genes for propionate kinase (*pduW*) and a threonine kinase involved in B_{12} synthesis (*pduX*) were identified elsewhere in the *A. longum* genome. The gene for NADPH-dependent propanol dehydrogenase (*pduQ*) was not identified specifically, but several homologs of unspecified alcohol dehydrogenases were found.

1,2-PD induces transcription and translation of PDU-associated genes. To check whether the appearance of the microcompartments correlated with expression of the PDU genes, the transcription of two PDU-associated genes was assessed using
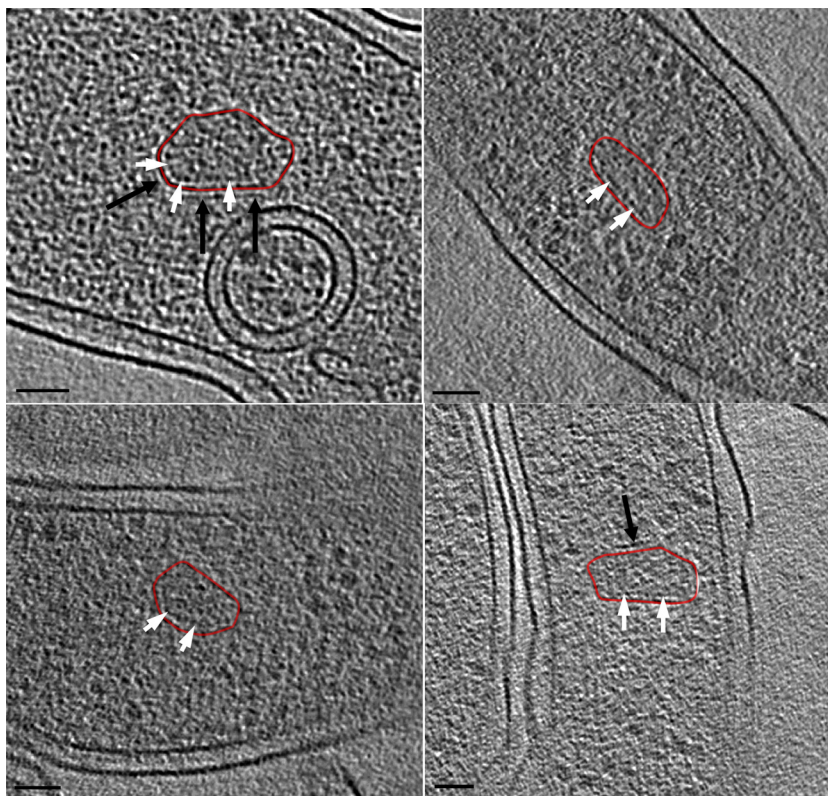
FIG 5 Organization of PDU microcompartments. The microcompartments appeared to be surrounded by a single layer of proteinaceous shell. Internal (white arrows) and external (black arrows) layers were also observed in some PDU microcompartments, alongside the protein shell (red contour). The continuous yet patchy appearance of the additional layers is likely indicative of some specific protein-protein interactions. Bars, 50 nm.

qRT-PCR. We focused on two *A. longum* genes, *pduU* and *pduC*, which are predicted to encode a structural PDU polyhedral body protein and the large subunit of the coenzyme B_{12}-dependent diol dehydratase, respectively. The levels of *pduU* and *pduC* transcripts detected at different time points depended on the specific carbon source added to the medium (Fig. 3A). Cells grown on glucose had low transcription levels of both genes at all time points investigated. As expected for PDU microcompartments, when cells were exposed to 1,2-PD, they responded rapidly by increasing transcription of *pduU* and *pduC*, by over 23- and 28-fold, respectively, within 24 h. While previous work has shown that, in *A. longum*, fermentation of fructose, mannose, mannitol, ribose, pyruvate, and oxaloacetate results in the production of butyrate and acetate (15), the major product of rhamnose fermentation was 1,2-PD (15). We therefore tested whether growth on rhamnose would result in transcription of *pduU* and *pduC*. Both genes were in fact strongly induced (approximately 18-fold and 20-fold increases, respectively), but only after 48 h of growth on rhamnose.

Cryotomograms of *A. longum* cells grown under the conditions described above were then recorded. No microcompartments were observed in cells grown on glucose after 24 and 48 h (*n* = 20), whereas growth on 1,2-PD for 24 h resulted in microcompartments in 5 of 7 cells. The majority of cells grown on rhamnose (33 of 36 imaged) lacked microcompartments after 24 h, but all the cells (*n* = 15) imaged after 48 h contained numerous microcompartments (Fig. 3B). We also tested whether growth on H_2 plus CO_2 alone could induce the synthesis of microcompartments. None of the 7 cells imaged after 48 h demonstrated the production

of microcompartments when these culture conditions were used. Because (i) the only microcompartment genes found in *A. longum* were clustered in a single operon closely resembling (in synteny and homology) the model PDU microcompartment genes of *S. enterica*, (ii) growth of *A. longum* cells in 1,2-PD or rhamnose resulted in expression of the putative PDU microcompartment genes, and (iii) transcription of these genes correlated with the appearance of the microcompartments, we concluded that the observed microcompartments were PDU microcompartments.

Structural features of PDU microcompartments. Like the other microcompartments previously observed, *A. longum* PDU microcompartments were seen to be thin-shelled irregular polyhedra. In cells grown on 1,2-propanediol, 2 to 6 microcompartments were seen in the 2- to 4-μm field of view of each cryotomogram, leading to an estimate of 35 to 210 microcompartments per ~70-μm cell. The size and shape of the intracellular PDU microcompartments (*n* = 40) were highly variable (Fig. 4). Manual segmentations of ~30 PDU microcompartments showed that the longest dimensions ranged from 80 to 200 nm, with surface areas ranging from 1,100 nm^2 to 3,100 nm^2 and volumes ranging from 2,900 nm^3 to 12,000 nm^3.

All the microcompartments were densely packed, presumably with enzymes involved in 1,2-PD degradation. No empty or partially assembled microcompartments were observed. In some cases, a layer of material was found just inside or outside the microcompartment shell, but not all the way around (Fig. 5), suggesting that the shell was composed of a single proteinaceous layer. The patchy appearance of the additional layers could be
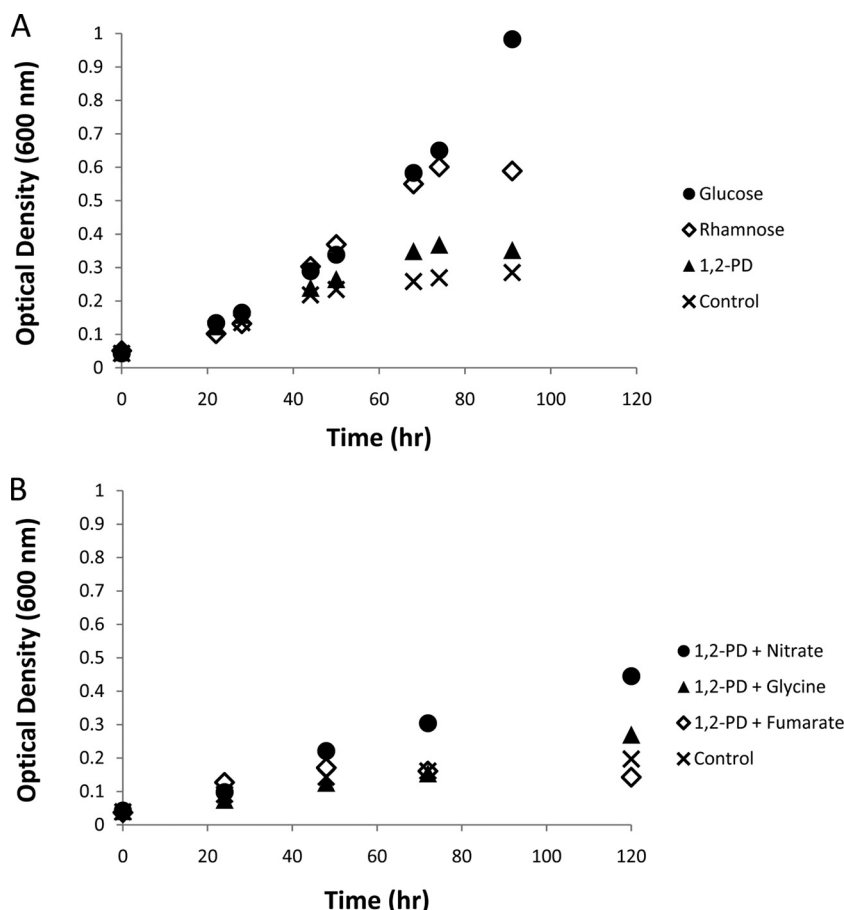
FIG 6 Growth of *A. longum* on different carbon sources (A) and with different terminal electron acceptors (B). (A) The cultures grew robustly when supplemented with either glucose or rhamnose. Growth on 1,2-PD was similar to that of the control, which received no additional carbon source. (B) The presence of nitrate as an electron acceptor stimulated growth above that of any of the other terminal electron acceptors tested and the control, which received neither 1,2-PD nor an exogenous terminal electron acceptor. None of these conditions resulted in an observed exponential growth phase.

indicative of some specific protein-protein interactions rather than a packing-induced order (11).

Growth of *A. longum* in different media. Compared to glucose or rhamnose, growth on 1,2-PD was dramatically slower and limited to much lower optical densities (Fig. 6A). An increase in optical density was observed when cells were grown on 1,2-PD and H_2 plus CO_2, but similar increases were observed for controls containing H_2 plus CO_2 with no additional organic carbon source. Because growth on 1,2-PD may depend on the presence of an appropriate terminal electron acceptor, various candidates were tested. Among these, nitrate supported stronger growth than glycine and fumarate (Fig. 6B). Tetrathionate was apparently lethal to *A. longum*, as evidenced by the cessation of growth and loss of motility in cultures shortly after addition of this chemical (the growth curve is not shown in Fig. 6B because tetrathionate also immediately oxidized the redox indicator resazurin, which was included in our medium to detect oxygen contamination, turning the culture pink and prohibiting optical density measurements).

DISCUSSION

Here we have shown that when starved or grown on certain sugars, *A. longum* synthesizes PDU microcompartments. In the termite gut, where *A. longum* is naturally found, cellulose hydrolysis and

subsequent fermentation of the released sugars are accomplished mainly by flagellate protozoa, which produce large amounts of CO_2 and H_2 in the process. Acetogenic bacteria such as *A. longum* then use these gasses to form acetate, thus contributing to the efficiency of the termite gut system by increasing the amount of acetate available for termite metabolism (29–31). In addition, it is known that *A. longum* can ferment fructose, mannose, mannitol, ribose, pyruvate, and oxaloacetate, resulting in the production of butyrate and acetate (15). The major product of rhamnose fermentation, however, is 1,2-PD (15). In *Salmonella enterica*, the presence of 1,2-PD induces the assembly of microcompartments, presumably to sequester the toxic by-products of 1,2-PD degradation (such as propionaldehyde) from the rest of the cytoplasm (12, 32–34). The possession and expression of PDU microcompartment genes by *A. longum* therefore suggest that *A. longum* is either sometimes involved in rhamnose fermentation or utilizes 1,2-PD that is otherwise available due to the breakdown of plant material within the termite gut (1). The absence of PDU microcompartments in cultures grown on glucose and the delayed assembly of PDU microcompartments in cultures grown on rhamnose (compared to growth on 1,2-PD directly) further suggest that sugars repress microcompartment assembly but that when these sugars are exhausted from the medium (for instance, before spo-

rulation is induced) and/or when 1,2-PD concentrations surpass a regulatory threshold, assembly begins (Fig. 3).

Like purified PDU microcompartments from *S. enterica* (35), *A. longum* PDU microcompartments are smaller and less regular than carboxysomes purified from *Synechococcus* species strain WH8102 (10). When carboxysomes were imaged in whole *Halothiobacillus neapolitanus* cells, some were only partially assembled (11). In those cases, a layer of RubisCO laid along the inner curvature of the unclosed shell. These observations are consistent with the results of a recent study which showed that the enzymes of the carboxysome microcompartment cluster together before they are encapsulated by the shell (8). While partially assembled PDU microcompartments were not observed in *A. longum*, our observation of a proteinaceous layer along the inner surface of some microcompartments points again to a coassembly mechanism. The consistent differences in shape and size of PDU microcompartments compared to carboxysomes may therefore be due to differences in the clustering properties of the enzymes they enclose, as well as to differences in the shell proteins.

ACKNOWLEDGMENTS

REFERENCES

1. **Kerfeld CA, Heinhorst S, Cannon GC.** 2010. Bacterial microcompartments. Annu. Rev. Microbiol. **64**:391–408. http://dx.doi.org/10.1146/annurev.micro.112408.134211.
2. **Yeates TO, Kerfeld CA, Heinhorst S, Cannon GC, Shively JM.** 2008. Protein-based organelles in bacteria: carboxysomes and related microcompartments. Nat. Rev. Microbiol. **6**:681–691. http://dx.doi.org/10.1038/nrmicro1913.
3. **Cannon GC, English RS, Shively JM.** 1991. In situ assay of ribulose-1,5-bisphosphate carboxylase/oxygenase in *Thiobacillus neapolitanus*. J. Bacteriol. **173**:1565–1568.
4. **Shively JM, Ball F, Brown DH, Saunders RE.** 1973. Functional organelles in prokaryotes: polyhedral inclusions (carboxysomes) of *Thiobacillus neapolitanus*. Science **182**:584–586. http://dx.doi.org/10.1126/science.182.4112.584.
5. **Shively JM, Ball FL, Kline BW.** 1973. Electron microscopy of the carboxysomes (polyhedral bodies) of *Thiobacillus neapolitanus*. J. Bacteriol. **116**:1405–1411.
6. **Tsai Y, Sawaya MR, Cannon GC, Cai F, Williams EB, Heinhorst S, Kerfeld CA, Yeates TO.** 2007. Structural analysis of CsoS1A and the protein shell of the *Halothiobacillus neapolitanus* carboxysome. PLoS Biol. **5**:e144. http://dx.doi.org/10.1371/journal.pbio.0050144.
7. **Tanaka S, Sawaya MR, Phillips M, Yeates TO.** 2009. Insights from multiple structures of the shell proteins from the beta-carboxysome. Protein Sci. **18**:108–120. http://dx.doi.org/10.1002/pro.14.
8. **Cameron JC, Wilson SC, Bernstein SL, Kerfeld CA.** 2013. Biogenesis of a bacterial organelle: the carboxysome assembly pathway. Cell **155**:1131–1140. http://dx.doi.org/10.1016/j.cell.2013.10.044.
9. **Tocheva EI, Li Z, Jensen GJ.** 2010. Electron cryotomography. Cold Spring Harb. Perspect. Biol. **2**:a003442. http://dx.doi.org/10.1101/cshperspect.a003442.
10. **Iancu CV, Ding HJ, Morris DM, Dias DP, Gonzales AD, Martino A, Jensen GJ.** 2007. The structure of isolated *Synechococcus* strain WH8102 carboxysomes as revealed by electron cryotomography. J. Mol. Biol. **372**:764–773. http://dx.doi.org/10.1016/j.jmb.2007.06.059.
11. **Iancu CV, Morris DM, Dou Z, Heinhorst S, Cannon GC, Jensen GJ.** 2010. Organization, structure, and assembly of alpha-carboxysomes determined by electron cryotomography of intact cells. J. Mol. Biol. **396**:105–117. http://dx.doi.org/10.1016/j.jmb.2009.11.019.
12. **Bobik TA, Havemann GD, Morris DM, Busch RJ, Williams DS, Aldrich HC.** 1999. The propanediol utilization (pdu) operon of *Salmonella enterica* serovar Typhimurium LT2 includes genes necessary for formation of polyhedral organelles involved in coenzyme B(12)-dependent 1,2-propanediol degradation. J. Bacteriol. **181**:5967–5975.
13. **Brinsmade SR, Paldon T, Escalante-Semerena JC.** 2005. Minimal functions and physiological conditions required for growth of Salmonella enterica on ethanolamine in the absence of the metabolosome. J. Bacteriol. **187**:8039–8046. http://dx.doi.org/10.1128/JB.187.23.8039-8046.2005.
14. **Sriramulu DD, Liang M, Hernandez-Romero D, Raux-Deery E, Lunsdorf H, Parsons JB, Warren MJ, Prentice MB.** 2008. *Lactobacillus reuteri* DSM 20016 produces cobalamin-dependent diol dehydratase in metabolosomes and metabolizes 1,2-propanediol by disproportionation. J. Bacteriol. **190**:4559–4567. http://dx.doi.org/10.1128/JB.01535-07.
15. **Kane MD, Breznak JA.** 1991. *Acetonema longum* gen. nov. sp. nov., an H_2/CO_2 acetogenic bacterium from the termite, *Pterotermes occidentis*. Arch. Microbiol. **156**:91–98. http://dx.doi.org/10.1007/BF00290979.
16. **Tocheva EI, Matson EG, Morris DM, Moussavi F, Leadbetter JR, Jensen GJ.** 2011. Peptidoglycan remodeling and conversion of an inner membrane into an outer membrane during sporulation. Cell **146**:799–812. http://dx.doi.org/10.1016/j.cell.2011.07.029.
17. **Altschul SF, Gish W, Miller W, Myers EW, Lipman DJ.** 1990. Basic local alignment search tool. J. Mol. Biol. **215**:403–410.
18. **Overbeek R, Begley T, Butler RM, Choudhuri JV, Chuang HY, Cohoon M, de Crecy-Lagard V, Diaz N, Disz T, Edwards R, Fonstein M, Frank ED, Gerdes S, Glass EM, Goesmann A, Hanson A, Iwata-Reuyl D, Jensen R, Jamshidi N, Krause L, Kubal M, Larsen N, Linke B, McHardy AC, Meyer F, Neuweger H, Olsen G, Olson R, Osterman A, Portnoy V, Pusch GD, Rodionov DA, Ruckert C, Steiner J, Stevens R, Thiele I, Vassieva O, Ye Y, Zagnitko O, Vonstein V.** 2005. The subsystems approach to genome annotation and its use in the project to annotate 1000 genomes. Nucleic Acids Res. **33**:5691–5702. http://dx.doi.org/10.1093/nar/gki866.
19. **Zheng SQ, Keszthelyi B, Branlund E, Lyle JM, Braunfeld MB, Sedat JW, Agard DA.** 2007. UCSF tomography: an integrated software suite for real-time electron microscopic tomographic data collection, alignment, and reconstruction. J. Struct. Biol. **157**:138–147. http://dx.doi.org/10.1016/j.jsb.2006.06.005.
20. **Kremer JR, Mastronarde DN, McIntosh JR.** 1996. Computer visualization of three-dimensional image data using IMOD. J. Struct. Biol. **116**:71–76. http://dx.doi.org/10.1006/jsbi.1996.0013.
21. **Leadbetter JR, Schmidt TM, Graber JR, Breznak JA.** 1999. Acetogenesis from H_2 plus CO_2 by spirochetes from termite guts. Science **283**:686–689. http://dx.doi.org/10.1126/science.283.5402.686.
22. **Graber JR, Leadbetter JR, Breznak JA.** 2004. Description of *Treponema azotonutricium* sp. nov. and *Treponema primitia* sp. nov., the first spirochetes isolated from termite guts. Appl. Environ. Microbiol. **70**:1315–1320. http://dx.doi.org/10.1128/AEM.70.3.1315-1320.2004.
23. **Krooneman J, Faber F, Alderkamp AC, Elferink SJ, Driehuis F, Cleenwerck I, Swings J, Gottschal JC, Vancanneyt M.** 2002. *Lactobacillus diolivorans* sp. nov., a 1,2-propanediol-degrading bacterium isolated from aerobically stable maize silage. Int. J. Syst. Evol. Microbiol. **52**:639–646. http://dx.doi.org/10.1099/ijs.0.01979-0.
24. **Toraya T, Honda S, Fukui S.** 1979. Fermentation of 1,2-propanediol with 1,2-ethanediol by some genera of Enterobacteriaceae, involving coenzyme B_{12}-dependent diol dehydratase. J. Bacteriol. **139**:39–47.
25. **Price-Carter M, Tingey J, Bobik TA, Roth JR.** 2001. The alternative electron acceptor tetrathionate supports B_{12}-dependent anaerobic growth of *Salmonella enterica* serovar Typhimurium on ethanolamine or 1,2-propanediol. J. Bacteriol. **183**:2463–2475. http://dx.doi.org/10.1128/JB.183.8.2463-2475.2001.
26. **Morris DM, Jensen GJ.** 2008. Toward a biomechanical understanding of whole bacterial cells. Annu. Rev. Biochem. **77**:583–613. http://dx.doi.org/10.1146/annurev.biochem.77.061206.173846.
27. **Bobik TA, Xu Y, Jeter RM, Otto KE, Roth JR.** 1997. Propanediol utilization genes (pdu) of *Salmonella typhimurium*: three genes for the propanediol dehydratase. J. Bacteriol. **179**:6633–6639.
28. **Cheng S, Fan C, Sinha S, Bobik TA.** 2012. The PduQ enzyme is an alcohol dehydrogenase used to recycle NAD+ internally within the Pdu microcompartment of *Salmonella enterica*. PLoS One **7**:e47144. http://dx.doi.org/10.1371/journal.pone.0047144.
29. **Breznak JA, Switzer JM.** 1986. Acetate synthesis from H(2) plus CO(2) by termite gut microbes. Appl. Environ. Microbiol. **52**:623–630.
30. **Pester M, Brune A.** 2007. Hydrogen is the central free intermediate during lignocellulose degradation by termite gut symbionts. ISME J. **1**:551–565. http://dx.doi.org/10.1038/ismej.2007.62.
31. **Breznak JA, Kane MD.** 1990. Microbial H_2/CO_2 acetogenesis in animal

Tocheva et al.

guts: nature and nutritional significance. FEMS Microbiol. Rev. **7:**309–313. http://dx.doi.org/10.1111/j.1574-6941.1990.tb01698.x.

32. **Sampson EM, Bobik TA.** 2008. Microcompartments for B_{12}-dependent 1,2-propanediol degradation provide protection from DNA and cellular damage by a reactive metabolic intermediate. J. Bacteriol. **190:**2966–2971. http://dx.doi.org/10.1128/JB.01925-07.

33. **Cheng S, Sinha S, Fan C, Liu Y, Bobik TA.** 2011. Genetic analysis of the protein shell of the microcompartments involved in coenzyme B_{12}-dependent 1,2-propanediol degradation by *Salmonella*. J. Bacteriol. **193:**1385–1392. http://dx.doi.org/10.1128/JB.01473-10.

34. **Cheng S, Bobik TA.** 2010. Characterization of the PduS cobalamin reductase of *Salmonella enterica* and its role in the Pdu microcompartment. J. Bacteriol. **192:**5071–5080. http://dx.doi.org/10.1128/JB.00575-10.

35. **Crowley CS, Sawaya MR, Bobik TA, Yeates TO.** 2008. Structure of the PduU shell protein from the Pdu microcompartment of *Salmonella*. Structure **16:**1324–1332. http://dx.doi.org/10.1016/j.str.2008.05.013.